

# Observation of the $4f^{14}6s^2\ ^1S_0 - 4f^{13}5d6s^2(J=2)$ clock transition at 431 nm in $^{171}\text{Yb}$

Akio Kawasaki,<sup>1,\*</sup> Takumi Kobayashi,<sup>1</sup> Akiko Nishiyama,<sup>1</sup> Takehiko Tanabe,<sup>1</sup> and Masami Yasuda<sup>1</sup>

<sup>1</sup>National Metrology Institute of Japan (NMIJ), National Institute of Advanced Industrial Science and Technology (AIST), 1-1-1 Umezono, Tsukuba, Ibaraki 305-8563, Japan

We report on the observation of the  $4f^{14}6s^2\ ^1S_0 - 4f^{13}5d6s^2(J=2)$  transition at 431 nm in  $^{171}\text{Yb}$  by depleting atoms in a magneto-optical trap formed by the  $6s^2\ ^1S_0 - 6s6p\ ^3P_1$  intercombination transition. The absolute frequency of the transition to the  $F=3/2$  state is determined to be 695 171 054 857.1(7.1) kHz against physical realisation of Coordinated Universal Time maintained by National Metrology Institute of Japan with a frequency comb. The  $g$  factor of the transition to the  $F=3/2$  state and the A hyperfine constant are measured to be 1.552(49) and 1123.273(12) MHz, respectively. Further precision spectroscopy of this transition can lead to new physics searches with isotope shift measurements, and a search for time variation of the fine structure constant.

Ytterbium (Yb) is one of the most popular atoms for the purpose of precision spectroscopy. Neutral atoms have two known narrow-linewidth transitions at 507 nm [1] and 578 nm [2], and  $\text{Yb}^+$  ions have three narrow linewidth transitions at 411 nm [3], 436 nm [4], and 467 nm [5]. These transitions, as well as some other broader transitions useful for specific applications, are precisely studied based on various motivations, such as operations of optical lattice clocks [6–12] and ion clocks [13, 14], searches for the time variation of fundamental constants [15], searches for ultralight dark matter [16–20], diagnosis of quantum degenerate gases [21, 22], searches for atomic parity violation [23], and searches for new physics with isotope shift measurements [24–27].

In addition to these transitions, two more narrow-linewidth transitions in neutral atoms are theoretically predicted to be beneficial for fundamental physics [28, 29]. The difference between these two transitions is the energy level for the lower-energy state, the  $6s^2\ ^1S_0$  ground state [28] and the  $6s6p\ ^3P_0$  state [29] that is typically known as the excited state for the clock transition at 578 nm, and they share the same excited state:  $[\text{Xe}]4f^{13}5d6s^2(J=2)$ . Because of its unusual electronic configuration where an electron in an inner-shell  $4f$  orbital is excited to a  $5d$  orbital, transitions connecting this  $4f^{13}5d6s^2(J=2)$  state and other (meta)stable states have some attractive features. One is high sensitivity to the variation of the fine structure constant, which is characterized by the sensitivity coefficient of  $K = -3.82$  for the  $4f^{14}6s^2\ ^1S_0 - 4f^{13}5d6s^2(J=2)$  transition [28] or  $K = -15$  for the  $4f^{14}6s6p\ ^3P_0 - 4f^{13}5d6s^2(J=2)$  transition [29]. This also improves the sensitivity to ultralight dark matter through its coupling to the fine structure constant [18–20, 30]. Another usage of this transition is new physics searches with isotope shift measurements. Because Yb has a large number of stable bosonic isotopes and various narrow-linewidth transitions in both neutral atoms and  $\text{Yb}^+$  ions, it is one of the most well studied atoms to search for new interaction between neutrons and electrons through isotope shift measurements [24–27]. One of the important factors for these searches is to utilize transitions including different electronic structures

to include a variety of distances between the nucleus and electrons, and the configuration of the  $4f^{13}5d6s^2(J=2)$  state differs from all other states involved in the transitions investigated so far. Also, high sensitivity to local Lorentz invariance is expected [28]. However, the transition to the  $4f^{13}5d6s^2(J=2)$  state is yet to be observed.

In this paper, we report the first observation of the 431 nm transition from the  $6s^2\ ^1S_0$  ground state to the  $4f^{13}5d6s^2(J=2)$  state in  $^{171}\text{Yb}$ . Specifically, the  $F=3/2$  hyperfine level, which has an enhancement of the transition rate by mixing of the electrical dipole transition due to nuclear spin in addition to the magnetic quadrupole (M2) transition, is carefully characterized. The absolute frequency and magnetic properties of the transition are determined.

The experimental apparatus was previously used for an optical lattice clock [31, 32]. Yb atoms emitted from an oven of  $\sim 880$  K are slowed down by a Zeeman slower and then trapped in a magneto-optical trap (MOT) generated by the  $6s^2\ ^1S_0 - 6s6p\ ^1P_1$  transition at 399 nm. Atoms are next transferred to the second-stage MOT formed with the  $6s^2\ ^1S_0 - 6s6p\ ^3P_1$  intercombination transition at 556 nm, where  $\sim 10^5\ ^{171}\text{Yb}$  atoms are trapped. After a cooling period, atoms are cooled down to 30  $\mu\text{K}$  and maintains its temperature through the period of interro-

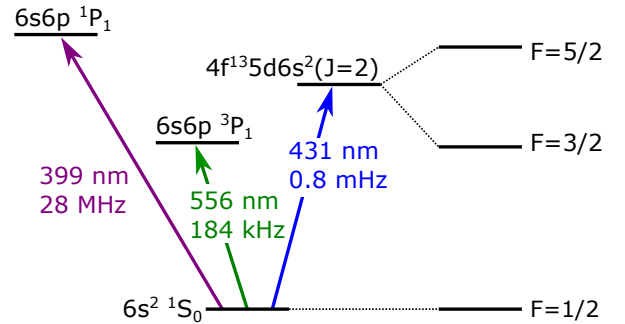


FIG. 1. Energy level in neutral  $^{171}\text{Yb}$  atom related to the search for the  $6s^2\ ^1S_0 - 4f^{13}5d6s^2(J=2)$  transition. The right most column shows hyperfine states for the ground state and the  $4f^{13}5d6s^2(J=2)$  state.

gation by the 431 nm light.

The 431 nm laser, which is subsequently sent onto the MOT, is generated by second harmonics generation with a waveguide periodically poled lithium niobate (PPLN) from a titanium sapphire (Ti:sapph) laser tuned at 862 nm. The 862 nm laser is locked to an ultrastable cavity through a fiber-laser-based frequency comb and a 1064 nm laser, whose short term relative stability is around  $2 \times 10^{-15}$  and long term stability is better than  $10^{-13}$  for averaging times of  $\lesssim 10^4$  s thanks to feedforward of the linear drift. Locking is performed with a slow feedback onto a piezoelectric actuator in the Ti:sapph laser and a fast feedback onto a double-pass acousto-optic modulator (AOM). The overall a bandwidth is  $\sim 100$  kHz, and locking narrows the linewidth of the laser down to  $\lesssim 1$  Hz, similar to the linewidth of the clock laser used in an Yb optical lattice clock [20, 33]. After the main output is sent to the PPLN module, it goes through another double-pass AOM for frequency tuning. The maximum attainable power of the 431 nm light at atoms is  $\sim 10$  mW with a beam size focused down to  $\sim 65 \mu\text{m}$   $e^{-2}$  radius. With the vertical axis defined as the  $z$  axis, the direction of the propagation of the incident 431 nm laser to the atoms is defined as the  $y$  axis, and the linear polarization of the 431 nm laser is aligned to the  $z$  axis.

The absolute frequency of the 431 nm laser is determined by precisely measuring the repetition frequency and carrier-envelope offset frequency of the frequency comb, which are at 53.148 319 MHz and 30 MHz, respectively, locked to the ultrastable cavity with a frequency counter referenced to a physical realisation of Coordinated Universal Time maintained by National Metrology Institute of Japan (UTC(NMIJ)). To reduce the measurement noise of the frequency counter, the repetition frequency is measured over  $\sim 1000$  s, during which different Zeeman shift measurements were performed. The mode number of the frequency comb is determined by using a wavemeter and an auxiliary frequency comb with a repetition frequency at 50.257 834 5 MHz locked to UTC(NMIJ) [34]. All other radiofrequency sources for generating frequency offsets between a mode in the frequency comb and the atomic resonance is referenced to UTC(NMIJ).

Fluorescence light from the MOT is recorded with a silicon photomultiplier (SiPM) and an amplifying circuit. To avoid any fluctuation of the amount of fluorescence by atoms or background scattering, the power of the 556 nm laser is stabilized by a servo circuit during the interrogation period.

The initial search for the  $4f^{14}6s^2\ ^1S_0 - 4f^{13}5d6s^2\ (J = 2)$  transition is performed with the 431 nm light shined onto the second-stage MOT while its frequency is scanned at the rate of 2 MHz/s by the double-pass AOM. This 1-s long scan is performed iteratively by shifting the scanning range at 1 MHz step. To cover scanning range larger than the modulation bandwidth for the double-

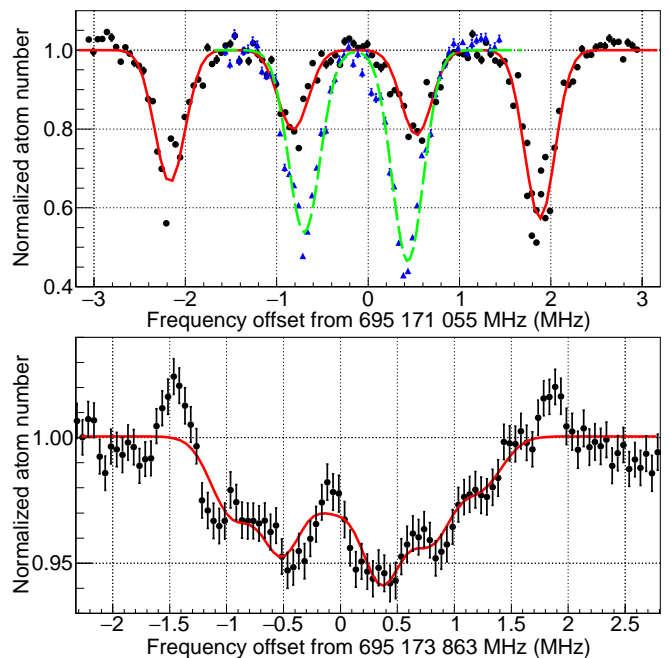


FIG. 2. Spectrum of the depletion of the MOT due to the  $4f^{14}6s^2\ ^1S_0 - 4f^{13}5d6s^2\ (J = 2)$  transition: (a) the  $F = 3/2$  hyperfine state. black circle (blue triangle) shows the spectrum with 0.62 (0.50) G magnetic field applied in the  $y$  ( $z$ ) direction. The red dotted (green dashed) curve is the fit of the black (blue) datapoints. (b) the  $F = 5/2$  hyperfine state. The red line shows the fit of the black points. The fitted center frequency is 0.142(27) MHz. The uncertainty includes the compensation of multiplying square root of  $\chi^2/\text{ndf} = 1.658$ . For all three curves, fits are performed with a constant offset and four (two, six) Gaussians are characterized by their common width, average detuning, spacing between adjacent dip that is regarded as the Zeeman splitting for  $\Delta|m_F| = 1$ , and four (two, six) independent amount of dips for the  $y$  field ( $z$  field,  $F = 5/2$ ). Systematic shifts are compensated.

pass AOM, the 431 nm laser is locked to different modes of the frequency comb. The signal of the resonance is the faster decrease in the atom number in the MOT compared to off-resonance cases. The  $F = 3/2$  hyperfine level is first observed with this scan, due to the stronger transition. The  $F = 5/2$  state is observed with substantially slower scanning rate of 200 kHz/s, because it is only allowed through the M2 transition.

Once the initial signature is observed for the  $F = 3/2$  hyperfine level, spectroscopy with the laser frequency fixed is performed. To eliminate the AC Stark shift and broadening due to the Zeeman effect, the second-stage MOT, both the 556 nm laser and the quadrupole magnetic field, is switched on and off for 40 times, and the 431 nm laser is sent for 3 ms each time while the MOT is off. To minimize the extra loss of atoms by accelerating atoms in a certain direction, the 556 nm laser is first instantaneously turned off by switching off an AOM and

then magnetic field is turned off. The ratio of the atom number after and before shining the pulses of the 431 nm laser is recorded. Each time the MOT is reloaded, the frequency of the 431 nm laser is decremented in a step of 50 kHz to obtain frequency dependent depletion ratios.

Figure 2 (a) shows an example spectrum. For the  $F = 3/2$  hyperfine levels, four dips corresponding to four different Zeeman sublevels for the excited state are observed when the bias magnetic field is applied in the  $y$  direction. Note that Zeeman splitting of the ground state in the order of 100 Hz is negligible in this precision. When the bias magnetic field is applied in the  $z$  direction, only  $\pi$  transitions are induced, and thus only two peaks are observed. In the most part of the estimates of the uncertainties below, the bias magnetic field  $B_z$  in the  $z$  direction is applied because the dip is deeper, and the bias magnetic field  $B_y$  in the  $y$  direction is applied in only a few cases. Prior to the measurements, splitting between the four dips is minimized by tuning bias coil current in the  $x$  and  $z$  direction to suppress residual magnetic field. When  $B_y$  ( $B_z$ ) is applied, obtained spectra are fitted with four (two) Gaussians and a constant offset.

Even if the four (two) Zeeman sublevels in the  $4f^{13}5d6s^2(J=2)$  state are not well separated, the fit performs reasonably well, and all data are used to obtain the average frequency of the four (two) resonant frequency, which is regarded as the resonant frequency for the  $F = 3/2$  hyperfine level of the  $4f^{14}6s^2\ ^1S_0 - 4f^{13}5d6s^2(J=2)$  transition. After taking average weighted by the standard deviation of different  $B_y$  ( $B_z$ ), the resonant frequency is determined with an uncertainty of 0.6 kHz. The major source of this fitting uncertainty presumably comes from the broadened peak of the transition due to atom's thermal motion. The smallest width of the peak corresponds to the Maxwell-Boltzmann distribution for 41  $\mu$ K. This is slightly higher than the typical temperature of atoms of 30  $\mu$ K measured by absorption imaging, and broader widths are also observed especially for large bias field, such as in Fig. 2 (a). Potential sources of the broadening are nonuniformity of the residual magnetic field and power broadening.

Other potential major sources of the uncertainty are the AC Stark shift due to the 431 nm light and the Doppler shift by potential kicking on the MOT at the moment of turning off the 556 nm laser. To test the AC Stark shift, the mean frequency of the two peaks when  $B_z$  is applied is measured for different power. The slope obtained from a linear fit gives 0.23(5.94) kHz shift for the 10 mW laser power, which is consistent with zero within the uncertainty. To evaluate the Doppler shift due to kicking on the MOT, the spectrum taken with 431 nm probe beam retroreflected is compared with the case without retroreflection. A shift of 12.8(3.5) kHz in the single beam case compared to the retroreflected case is observed. With finer scanning with 1 kHz step, Doppler

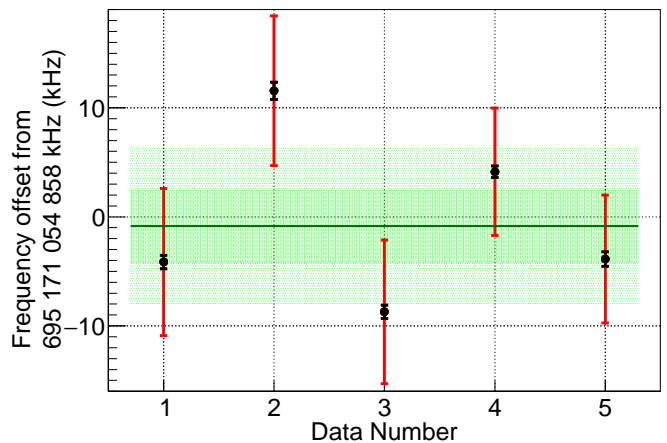


FIG. 3. Absolute frequency measurement of the  $4f^{14}6s^2\ ^1S_0 - 4f^{13}5d6s^2(J=2)$  transition: the black part of the error bars show the statistical uncertainty, and red part is the total uncertainty including systematic uncertainties. Green line is the average of five points weighted by the statistical uncertainty. Because  $\chi^2/\text{ndf} = 137.3$ , the uncertainty of the fit is multiplied by  $\sqrt{\chi^2/\text{ndf}}$ , which is shown in the dark green band. Light green band is the total uncertainty including the systematic uncertainties. Obtained average in the plot is  $-0.87 \pm 3.28(\text{stat}) \pm 6.32(\text{syst})$  kHz.

free doublet is observed. The average frequency of this pair and the average of the gaussian fit obtained in the spectroscopy with 50 kHz step is 3.3(4) kHz different, and thus conservatively, 3.3 kHz is added to the uncertainty due to the Doppler shift.

With these major sources of uncertainty, other uncertainties and systematic shifts are negligible. The relative uncertainty of the frequency measurement of the 431 nm laser arising from the measurement noise of the frequency counter around  $10^{-13}$  at 1000 s average time, which is in the same order of magnitude as the overall data acquisition time for the data used for the resonant frequency measurement, is well below 1 kHz. The relative uncertainty of UTC(NMIJ) is confirmed to be less than  $10^{-14}$  by comparing UTC(NMIJ) with International Atomic Time via a satellite link. Other systematic effects on atoms, such as the 2nd order Zeeman shift, the black body radiation shift, the DC and AC Stark shift, and the collisional shift typically appear on the level of 1 Hz or less and thus negligible here. Particularly, it should be noted that the 2nd order Zeeman shift is predicted to be a few Hz/G<sup>2</sup> theoretically [28], and this justifies the simple assumption that the Zeeman splitting between adjacent  $m_F$  states is the same for all  $m_F$  in the  $\sim 1$  kHz accuracy. The noise added to the laser during the transmission of the undoubled 431 nm light through an optical fiber is estimated to be in the order of  $10^{-15}$ , which is negligible compared to the major source of uncertainty.

Combining these shifts and uncertainties, the absolute frequency is derived from several data shown in

Fig. 3. Obtained average absolute frequency of the transition from the  $4f^{14}6s^2\ ^1S_0$  ground state to the  $F = 3/2$  hyperfine level of the  $4f^{13}5d6s^2(J = 2)$  state is 695 171 054 857.1 kHz. Because the fluctuation of the data around the weighted average is substantially larger than their statistical uncertainties,  $\sqrt{\chi^2/\text{ndf}}$  (ndf: number of degrees of freedom) is multiplied to the uncertainty for the weighted average to obtain overall statistical uncertainty. It should be noted that the underestimation of the statistical uncertainty at least partially comes from somewhat strange statistical behavior of the SiPM detector, and thus the same compensation is performed for the AC Stark shift, Doppler shift, and  $g$  factor evaluations. Together with the systematic uncertainty of 6.3 kHz, overall uncertainty is estimated to be 7.1 kHz. This number corresponds to 23 188.410 392 14(24)  $\text{cm}^{-1}$ , which has a reasonable agreement with previously reported number of 23188.518  $\text{cm}^{-1}$  [35, 36]. The uncertainty improved at least four orders of magnitude, and the difference can be explained by an isotope shift.

To determine the Landé's  $g$  factor for the  $4f^{14}6s^2\ ^1S_0 - 4f^{13}5d6s^2(J = 2)$  transition, bias magnetic field  $B_z$  in the  $z$  direction is applied to measure the frequency difference between a pair of  $\pi$  transitions between  $m_F = \pm 1/2$  states. This configuration is more reliable than bias magnetic fields in the  $x$  or  $y$  directions, because the amount of magnetic field is calibrated not only by a Hall probe but also with the  $6s^2\ ^1S_0 - 6s6p\ ^3P_0$  clock transition [32]. In fact, the number obtained in Ref. [32] matches with reports from other setups [6, 37] at  $\lesssim 1\%$  level, and thus the uncertainty of the calibration of magnetic field is estimated to be 1%. Fig. 4 shows the amount of the splitting between these two  $\pi$  transitions for different bias field. The data is fitted with  $\Delta f_{\text{Zeeman}} = g\mu_B\sqrt{B_z^2 + B_\perp^2}$ . The obtained Landé's  $g$ -factor is 1.552(49), which has a reasonable agreement with a theoretical prediction of 1.5 [28].

As for the  $F = 5/2$  hyperfine state, the transition rate obtained in the setup described in this manuscript is too small to perform the characterization with MOT light off described for the  $F = 3/2$  hyperfine state. Instead, the 431 nm light with a fixed frequency is kept on for 1 s without turning off the MOT. The ratio of the atom number after and before the 1 s irradiation of the 431 nm is plotted for different frequencies in Fig. 2(b). Note that the plot is an average of two scans, with smoothing by averaging five adjacent frequency. The plot is fitted with a constant offset and six Gaussians, and the mean frequency of the six peaks is regarded as the best estimate for the transition frequency. An additional systematic shift here is the AC Stark shift due to the 556 nm laser. This is separately estimated with the  $F = 3/2$  hyperfine state to be 0.1018(78) MHz. The absolute frequency of the  $F = 5/2$  state is therefore determined to be 695 173 863 163(30) kHz. The hyperfine splitting for the  $^{171}\text{Yb}$  is estimated to be 2 808.183(31) MHz, and thus the

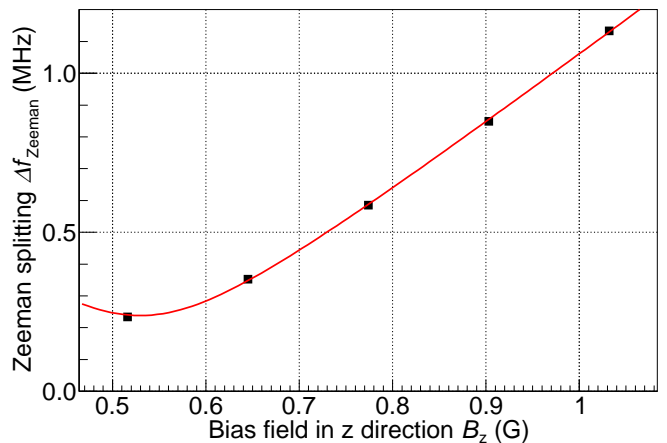


FIG. 4. Amount of Zeeman splitting for  $\Delta|m_F| = 1$  under different bias magnetic field: the red curve is the fit of black points by  $\Delta f_{\text{Zeeman}} = g\mu_B\sqrt{B_z^2 + B_\perp^2}$ , where  $g$  and  $B_\perp = \sqrt{B_x^2 + B_y^2}$  are fitted parameters. The best fit provides  $g = 1.552(46)$  and  $B_\perp = 0.1084(54)$  G. Uncertainties shown here is statistical only, and include the compensation by the square root of  $\chi^2/\text{ndf} = 6.01$ .

A hyperfine constant, which is defined by the magnetic dipole Hamiltonian of  $\hat{H}_D = \hat{A}\mathbf{I} \cdot \mathbf{J}$  with  $\mathbf{I}$  being nuclear spin and  $\mathbf{J}$  being total electronic angular momentum, is determined to be 1123.273(12) MHz.

To summarize, we observed the  $4f^{14}6s^2\ ^1S_0 - 4f^{13}5d6s^2(J = 2)$  clock transition at 431 nm in  $^{171}\text{Yb}$ , and determined its transition frequency to the  $F = 3/2$  hyperfine state as 695 171 054 857.1(7.1) kHz. This transition has a  $g$  factor of 1.552(49), and the hyperfine A constant is measured to be 1123.273(12) MHz. Further investigation of the transition has various significances on fundamental physics, such as new physics search with isotope shift measurements, dark matter search with clock comparison, and search for time variation of the fundamental constants. For these purposes, more precise spectroscopy is essential. The standard path for this taken in other clock transitions is to trap atoms in an optical lattice for interrogation in Lamb-Dicke regime, and to find a magic wavelength for AC Stark shift free spectroscopy for  $< 1$  Hz accuracy. Particularly for the new physics search with isotope shift measurements, determination of the isotope shift at this precision is important.

This work was supported by JSPS KAKENHI 21K20359, 22H01161, 22K04942, JST FOREST JP-MJFR212S, JST-MIRAI JPMJM118A1, and Research Foundation for Opto-Science and Technology. We are grateful to D. Akamatsu, K. Hosaka, H. Inaba, and S. Okubo for the development of the frequency comb and the ultrastable laser at 1064 nm.

*Note added*—While we are finalizing the manuscript, we noticed another report of the observation of the same transition [38].

- 
- \* [akio.kawasaki@aist.go.jp](mailto:akio.kawasaki@aist.go.jp)
- [1] A. Yamaguchi, S. Uetake, and Y. Takahashi, *Appl. Phys. B* **91**, 57 (2008).
- [2] C. W. Hoyt, Z. W. Barber, C. W. Oates, T. M. Fortier, S. A. Diddams, and L. Hollberg, *Phys. Rev. Lett.* **95**, 083003 (2005).
- [3] P. Taylor, M. Roberts, S. V. Gateva-Kostova, R. B. M. Clarke, G. P. Barwood, W. R. C. Rowley, and P. Gill, *Phys. Rev. A* **56**, 2699 (1997).
- [4] D. Engelke and C. Tamm, *Europhys. Lett.* **33**, 347 (1996).
- [5] M. Roberts, P. Taylor, G. P. Barwood, P. Gill, H. A. Klein, and W. R. C. Rowley, *Phys. Rev. Lett.* **78**, 1876 (1997).
- [6] W. F. McGrew *et al.*, *Nature* **564**, 87 (2018).
- [7] T. Kobayashi, D. Akamatsu, K. Hosaka, Y. Hisai, M. Wada, H. Inaba, T. Suzuyama, F.-L. Hong, and M. Yasuda, *Metrologia* **57**, 065021 (2020).
- [8] H. Kim, M.-S. Heo, C. Y. Park, D.-H. Yu, and W.-K. Lee, *Metrologia* **58**, 055007 (2021).
- [9] M. Pizzocaro, F. Bregolin, P. Barbieri, B. Rauf, F. Levi, and D. Calonico, *Metrologia* **57**, 035007 (2020).
- [10] A. Zhang *et al.*, *Metrologia* **59**, 065009 (2022).
- [11] N. Nemitz, T. Ohkubo, M. Takamoto, I. Ushijima, M. Das, N. Ohmae, and H. Katori, *Nat. Photonics* **10**, 258 (2016).
- [12] L. Luo *et al.*, *Metrologia* **57**, 065017 (2020).
- [13] N. Huntemann, C. Sanner, B. Lipphardt, C. Tamm, and E. Peik, *Phys. Rev. Lett.* **116**, 063001 (2016).
- [14] C. F. A. Baynham *et al.*, *J Mod. Opt.* **65**, 585 (2018).
- [15] R. Lange, N. Huntemann, J. M. Rahm, C. Sanner, H. Shao, B. Lipphardt, C. Tamm, S. Weyers, and E. Peik, *Phys. Rev. Lett.* **126**, 011102 (2021).
- [16] C. J. Kennedy, E. Oelker, J. M. Robinson, T. Bothwell, D. Kedar, W. R. Milner, G. E. Marti, A. Derevianko, and J. Ye, *Phys. Rev. Lett.* **125**, 201302 (2020).
- [17] A. Hees, J. Guéna, M. Abgrall, S. Bize, and P. Wolf, *Phys. Rev. Lett.* **117**, 061301 (2016).
- [18] M. Filzinger, S. Dörscher, R. Lange, J. Klose, M. Steinle, E. Benkler, E. Peik, C. Lisdat, and N. Huntemann, (2023), [arXiv:2301.03433](https://arxiv.org/abs/2301.03433) [physics.atom-ph].
- [19] N. Sherrill *et al.*, (2023), [arXiv:2302.04565](https://arxiv.org/abs/2302.04565) [physics.atom-ph].
- [20] T. Kobayashi *et al.*, *Phys. Rev. Lett.* **129**, 241301 (2022).
- [21] A. Yamaguchi, S. Uetake, D. Hashimoto, J. M. Doyle, and Y. Takahashi, *Phys. Rev. Lett.* **101**, 233002 (2008).
- [22] H. Konishi, F. Schäfer, S. Ueda, and Y. Takahashi, *New J Phys.* **18**, 103009 (2016).
- [23] D. Antypas, A. Fabricant, J. E. Stalnaker, K. Tsigutkin, V. V. Flambaum, and D. Budker, *Nat. Phys.* **15**, 120 (2019).
- [24] J. Hur *et al.*, *Phys. Rev. Lett.* **128**, 163201 (2022).
- [25] I. Counts, J. Hur, D. P. L. Aude Craik, H. Jeon, C. Leung, J. C. Berengut, A. Geddes, A. Kawasaki, W. Jhe, and V. Vuletić, *Phys. Rev. Lett.* **125**, 123002 (2020).
- [26] N. L. Figueroa, J. C. Berengut, V. A. Dzuba, V. V. Flambaum, D. Budker, and D. Antypas, *Phys. Rev. Lett.* **128**, 073001 (2022).
- [27] K. Ono, Y. Saito, T. Ishiyama, T. Higomoto, T. Takano, Y. Takasu, Y. Yamamoto, M. Tanaka, and Y. Takahashi, *Phys. Rev. X* **12**, 021033 (2022).
- [28] V. A. Dzuba, V. V. Flambaum, and S. Schiller, *Phys. Rev. A* **98**, 022501 (2018).
- [29] M. S. Safronova, S. G. Porsev, C. Sanner, and J. Ye, *Phys. Rev. Lett.* **120**, 173001 (2018).
- [30] A. Arvanitaki, J. Huang, and K. Van Tilburg, *Phys. Rev. D* **91**, 015015 (2015).
- [31] T. Kohno, M. Yasuda, K. Hosaka, H. Inaba, Y. Nakajima, and F.-L. Hong, *Appl. Phys. Express* **2**, 072501 (2009).
- [32] M. Yasuda *et al.*, *Appl. Phys. Express* **5**, 102401 (2012).
- [33] H. Inaba, K. Hosaka, M. Yasuda, Y. Nakajima, K. Iwakuni, D. Akamatsu, S. Okubo, T. Kohno, A. Onae, and F.-L. Hong, *Opt. Express* **21**, 7891 (2013).
- [34] R. Holzwarth *et al.*, *Applied Physics B* **73**, 269 (2001).
- [35] S. Ahmad, I. Machado, and G. Saksena, *Spectrochim. Acta Part B* **35**, 215 (1980).
- [36] A. Kramida, Yu. Ralchenko, J. Reader, and NIST ASD Team, NIST Atomic Spectra Database (ver. 5.10), [Online]. Available: <https://physics.nist.gov/asd> [2023, February 22]. National Institute of Standards and Technology, Gaithersburg, MD. (2022).
- [37] X. Zhang *et al.*, *Laser Physics Letters* **12**, 025501 (2015).
- [38] T. Ishiyama, K. Ono, T. Takano, A. Sunaga, and Y. Takahashi, (2023), [arXiv:2303.09765](https://arxiv.org/abs/2303.09765) [physics.atom-ph].